JOURNAL OF BEHAVIORAL HEALTH, 2025
VOL 14, NO. 3, PAGE 1 – 11

RESEARCH ARTICLE

Open Access

Expression and Distribution of Calcium-Proteins Binding in Cultured Human Lens Epithelial Cells *In Vitro* and in the Lens of Selenium Cataract Sprague-Dawley Rat *In Vivo*

Liu Kang[2] and Yu Geng[1]*

[1]Department of Ophthalmology, Hospital of Kunming Medical University, Kunming 650031, Yunnan province, People's Republic of China.
[2]Department of Ophthalmology, The 920th Hospital of the Joint Logistics Support Force, Kunming 650032, Yunnan Province, People's Republic of China.

ABSTRACT

Purpose: To investigate the pathogenesis of age-related cataract, we aim to examine the expression and distribution of Calb1 in cultured human lens epithelial cells (HLECs) subjected to calcium overload *in vitro*, as well as in the lenses of selenium-induced cataract SD rats *in vivo*.

Methods: The human lens epithelial cell line (SRA01/04) was treated with ionomycin at concentrations of 0.5 µmol/L, 1.0 µmol/L, 1.5 µmol/L, and 2.0 µmol/L for 1 hour to induce intracellular calcium overload in order to determine the optimal treatment concentration. Cell morphology changes were observed under an inverted microscope, cell viability was assessed using CCK-8 assay, intracellular calcium concentration was measured using a fluorescence microplate reader, and the distribution of calcium ions was visualized through confocal microscopy in HLECs labeled with Fluo-4/AM fluorescent probe at time points of 6 h, 12 h, 24 h, and 48 h post-treatment. Immunohistochemistry and Western Blot analysis were used to locate and quantify CALB1 protein expression levels while qRT-PCR was used to detect Calb1 mRNA expression levels in cultured HLECs as well as in the lenses of selenium cataract SD rats. Statistical comparisons were performed using one-way ANOVA followed by independent sample t-test.

Results: A treatment concentration of 1.0 µM ionomycin was determined as optimal. Between 6h and 12h, cell viability reached its lowest point while intracellular Ca^{2+} concentration peaked. Subsequently, cell viability gradually increased from 24h to 48h, while intracellular Ca^{2+} concentration remained stable and low. Upon calcium overload, the number of Calb1 spots decreased at 6h before increasing at 12h and becoming concentrated near the nucleus without a distinct pattern by 24h. At 48h, both fluorescence intensity and range expanded compared to that observed at 24 h. In selenium-induced cataractous lenses of SD rats, CALB1 protein gradually increased from 2 w to 8 w with prominent localization within the internal nucleus region at 12 w. qRT-PCR revealed that Calb1 mRNA expression significantly increased after calcium overload with peak expression occurring at 48h ($p<0.01$). Similarly, in selenium cataract SD rats, Calb1 mRNA expression was significantly higher compared to control groups from 4w to 12w ($p<0.01$), peaking at 8w before slightly decreasing by 12w. Western Blot demonstrated that following calcium overload there was no change in relative CALB1 protein expression within each time point for control groups; however, it significantly increased after calcium overload with peak expression occurring at 48 h ($p<0.01$) for experimental groups while lens CALB1 protein decreased significantly 2-week post-selenium induction but then increased 4-week post-induction before being highly expressed during 8w and 12w.

Conclusion: The CALB1 protein is mainly found in the cytoplasm of HLECs and the perinuclear region of lens fibers. After calcium overload, Calb1 may play a crucial role in reducing and stabilizing intracellular Ca^{2+} levels, protecting the lens from oxidative damage and promoting transparency.

ARTICLE HISTORY

Received Date: 20 Mar 2025
Accepted Date: 29 Apr 2025
Published Date: 07 May 2025

KEYWORDS

Calcium ion binding protein (Calb1), Age-related cataract, Human lens epithelial cells (HLEC), Selenium cataract SD rat model, Calcium ions.

Contact: Yu Geng, Department of Ophthalmology, Hospital of Kunming Medical University, Kunming 650031, Yunnan province, People's Republic of China.

Introduction

Age-related cataract represents a significant global burden of visual impairment and blindness [1]. Previous studies on age-related cataract have primarily focused on the external changes in lens proteins, often overlooking the exploration of cellular-level alterations and their underlying molecular mechanisms. Therefore, investigating the dynamic changes in lens protein within cells and comprehensively understanding the pathogenesis of age-related cataract at a molecular level will provide valuable insights for developing effective strategies to prevent and treat this condition.

Intracellular and extracellular calcium balance is a crucial prerequisite for maintaining normal cellular function and information transmission. Calcium ions play pivotal roles in numerous physiological processes within the body, including the nervous system, synthesis and release of neurotransmitters, axoplasmic transport, excitatory changes of cell membranes, as well as memory formation and other vital physiological activities [2-10]. The distribution of calcium ions both inside and outside the cell is often regulated by calcium ion binding protein (Calb1), in addition to the involvement of calcium ion channels present on the cell membrane [2].

Calb1 belongs to the calcium ion binding protein family in the EF-Hand domain, with a molecular weight of approximately 28,000 Daltons [11]. It was initially discovered in the small intestinal mucosa of chickens during the 1960s [12], and its expression level in tissues is regulated by 1,25-dihydroxy vitamin D3. Apart from the small intestinal mucosa, Calb1 is also expressed in various other tissues including kidney [13], brain [14], cerebellum [15], pancreas [16], and bone tissue [17,18].

Calb1, a calcium ion-regulated key buffer protein, exhibits reduced expression in various age-related tissue and organ diseases, leading to cellular calcium imbalance and increased intracellular free calcium ions, ultimately resulting in cell damage. Moreover, Calb1 activates Ca^{2+}/Mg^{2+}-ATPase activity and prevents excessive accumulation of calcium ions.

In recent years, research on Calb1 has primarily focused on its role in the nervous system. Numerous studies have demonstrated a correlation between abnormal calcium regulation mediated by Ca^{2+} binding protein and various human diseases, including hypertension, neurodegenerative diseases, and tumors [19-21]. The aberrant expression and distribution of Ca^{2+} binding protein may contribute to the development of these diseases. In an aged rat model, the expression level of Calb1 mRNA was found to be reduced by 60% ~ 80% throughout the entire brain, with a more pronounced decrease observed in the cerebellum, striatum, and brain stem [22]. Similarly, elderly individuals with neurodegenerative diseases exhibited a decline in brain Calb1 levels ranging from 60% to 88%. Recent investigations have also revealed that besides its role as a calcium buffer, Calb1 exerts anti-apoptotic effects on nerve cells [23-25].

The primary mechanism underlying cataract formation induced by sodium selenite involves calcium overload and oxidative damage [26], which partially mirrors the pathological changes observed in age-related cataracts [27]. Consequently, the selenium-induced cataract model in SD rats currently represents an ideal animal model for simulating senile cataracts [28-31].

However, the expression of Calb1 in HLECs following calcium ion overload and its dynamic changes during the onset and progression of selenium-induced cataract in SD rats have not been previously documented.

The objective of this study was to establish a theoretical and experimental foundation for understanding the pathogenesis of age-related cataract by conducting morphological observations and quantitative analysis on the expression and distribution of Calb1 *in vitro* using HLECs with calcium ion overload, as well as *in vivo* using lenses from SD rats with selenium-induced cataract.

Literature Review and Methods

Cells and Animals

The Animal Ethics Committee of the First Affiliated Hospital of Kunming Medical University approved all experiments conducted in accordance with the ethical code of the Committee for the Management and Use of Laboratory Animals. SD rats were sourced from Zhongshan Ophthalmology Center's experimental animal center. The human lens epithelial cell line (SRA01/04) was provided by Kunming Medical University. For selenium cataract experiments, suckling SD rats aged 8-12 d were used as experimental animals. At 2, 4, 8, and 12 w after modeling, rats were anesthetized with intraperitoneal injection of 10% chloral hydrate before immediate removal of their eyes. Cryopreserved SRA01/04 cells stored in liquid nitrogen were resuscitated and sub cultured for subsequent experiments.

Refinement of a Calcium Overload Model in HLECs

After autoclaving polyline - coated cover slides (12 mm × 12 mm, 0.17 mm thick), they were placed in 12-well plates and a cell suspension of 2.5×10^5 cells/mL was added to each well with the cover slide. Alternatively, for the 96-well plate experiment, a cell suspension of 3×10^4 cells/mL (100 µL) was added to each well. The plates were then incubated for 24-48 h until the cells adhered and covered at least 70%-80% of the bottom surface area. Subsequently, only culture medium was added to the control group while culture medium containing ionomycin (Sigma, USA), with concentrations ranging from 0.5 µmol/L to 2.0 µmol/L, was added to the experimental groups. The cultured HLECs underwent three washes with Hank's solution at different time points (1 h, 6 h, 12 h, 24 h, and 48 h). Fluo-4/AM working solution and Pluronic F127 (0.05%) were then added in a volume of either 250 µL per well for the12-well plate or 10 µL per well for the 96-well plate. The plates were incubated for 30 min in a controlled environment. To ensure complete removal of extracellular residual Fluo-4/AM, the Ca^{2+}-overloaded HLECs underwent three additional washes with Hank's solution.

Cell Viability of HLECs Following Calcium Overload

At 1h, 6h, 12h, 24h, and 48h, a Cell Counting Kit-8 (CCK-8)

solution of 10 µL was added to each well of the overloaded Ca^{2+}-treated HLEC-containing wells in a 96-well plate. The plate was then incubated for 2 h before measuring the absorbance at 450 nm using a microplate reader.

Quantification of Ca^{2+} concentration in HLECs following Calcium Overload

The 96-well plate containing overloaded HLECs was shielded from light at 1h, 6h, 12h, 24h, and 48h time points. Subsequently, the fluorescence intensity of cells located at the bottom of the plate was measured using a fluorescent enzyme reader with an excitation wavelength of 494 nm and an emission wavelength of 516 nm.

Revealing Intracellular Ca^{2+} Distribution Through Confocal Microscopy

The intracellular distribution of Ca^{2+} was visualized using a 40× oil immersion microscope, employing excitation light at 488 nm and imaging with a Zeiss LSM 510 confocal microscope.

Immunohistochemistry for Cultured HLECs *in vitro*

The SRA01/04 cell suspension (500 µl, approximately 2.5×10^5 cells/ml) was added to a well with a polyline - coated cover slide. The plates were then incubated in a cell incubator for 24 h until the cells adhered and proliferated on the surface. Immunofluorescence staining was performed using a cover slide that covered about 80% of the cellular area.

The medium was removed from the plates and rinsed with sterilized 0.01 M PBS solution at 37°C three times, each lasting for 5 min. Subsequently, the following procedures were conducted: fixation with 4% paraformaldehyde for 20 min, enhancement of cell permeability using 50 µL of 0.1% Triton X-100 (Beyotime, China) for half an hour, addition of approximately 25 µL (1:2000 dilution) rabbit anti-CalB1 primary antibody (Merck Millipore, USA) to cover the well bottom, and overnight storage in a refrigerator at a temperature of 4°C. Between each step, the wells were washed thrice with sterilized PBS solution (0.01 M) for 5 min each time.

Subsequently, fluorescent secondary antibody (Abcam, UK) diluted at ratio of 1:500 was added into each well followed by incubation at a temperature of 37°C for 1 h; Hoechst dye (Beyotime, China) was used to stain cell nuclei for five minutes; finally, anti-quench sealing tablets were applied to seal the samples. Again, between each mentioned step above, washing was carried out thrice with sterilized PBST solution containing a concentration of 0.01M per wash cycle lasting 5 min before proceeding to subsequent steps. Finally, the images were observed and collected using confocal microscopy.

Immunohistochemistry for Frozen Section of Lens

The SD rats were anesthetized with a 5% chloral hydrate injection and fixed by systemic infusion of 4% paraformaldehyde. After removing the eyeball, a small incision (about 1 ~ 3mm) was made at the limbus. The eyeball was then immersed in a 4% paraformaldehyde solution dissolved in a pH 7.2 PB solvent for 4 h. Subsequently, the eyeball underwent dehydration using successive sucrose solutions of increasing concentrations (10%→20%→30%). The lens was carefully removed, embedded in OCT, sliced into thin sections (5 ~ 10µm) using a frozen microtome, and finally baked at 55°C for 2 h.

The SD rats were anesthetized with a 5% chloral hydrate intraperitoneal injection and fixed by systemic infusion of 4% paraformaldehyde. After completely extracting the eyeball, a puncture incision measuring approximately 1 ~ 3 mm was made at the limbus. Subsequently, the eyeball was immersed in a solution containing 4% paraformaldehyde dissolved in pH 7.2 PB solvent (0.1 M) for 4 h. Afterwards, the eyeball underwent successive immersion in sucrose solutions ranging from 10% to 30% for dehydration. Careful removal of the lens was performed, followed by embedding it in OCT and slicing into sections measuring between 5 ~ 10 µm using a frozen microtome. Finally, these sections were baked at 55°C for 2 h.

The sections were rinsed three times with a 0.01 M pH 7.2 ~ 7.4 PBS solution for 5 min each. Endogenous peroxidase activity was blocked by treating the sections with 3% H_2O_2 in the dark for 30 min. After rinsing the sections three times with PBS solution for 5 min each, they were incubated in a wet box at either room temperature for 1 h or at 37°C for 30 min after adding a solution of normal goat serum (5%). Calb1 primary antibody solution (dilution range: 1:1000 ~ 1:2000) was added and refrigerated overnight at 4°C, followed by rinsing the sections three to five times with a PBST solution (0.01 M). Subsequently, PV-9000 reagent I was added and incubated at 37°C for 30 min, then rinsed again three times with PBST solution (0.01 M) for 5 min each time. PV-9000 reagent II was added and incubated under the same conditions as before, followed by another round of rinsing five times with PBST solution (0.01 M) for 5 min each time. Following the instructions in the DAB color kit chamber, the color development step proceeded at room temperature for 5 min before termination with double steamed water treatment. Hematoxylin staining was applied for nucleus staining, followed by differentiation using alcohol hydrochloride. Eosin staining saturated with $NaHCO_3$ stained cytoplasmic components blue within 10 min. Excess water on slides was eliminated by blotting with filter papers before dehydrating them through successive immersion in increasing concentrations of gradient alcohols (70%, 80%, 85%, 90%, 95% and finally, pure alcohol). Alternatively, oven drying could be used. The specimens were immersed sequentially in Xylene I and Xylene II for a total of 15 min to achieve transparency. After sealing with neutral resin and air-drying under a fume hood for 48 h, images were captured using an ordinary light microscope.

qRT-PCR

The rat Calb1 and glycolysis glyceraldehyde 3-phosphate dehydrogenase (GAPDH) sequences were retrieved using the BLAST tool from http://www.ncbi.nlm.nih.gov. Subsequently, Primer 5.0 software was used to design the gene primers for Calb1 and GAPDH. For selenium cataract SD rats and humans, Guangzhou Yingjie synthesized the Calb1 primers (refer to Table 1, Table 2).

Table 1: Primer design for qRT-PCR.

Genes(rat)	Forward primer	Reverse primer
Rat-Calb1 (116bp)	ACACTGACCACAGTGGCTTC	GTTCGGTACAGCTTCCCTCC
Rat-GAPDH (129bp)	TGCCACTCAGAAGACTGTGG	TTCAGCTCTGGGATGACCTT

Table 2: Primer design for qRT-PCR.

Genes (Human)	Forward primer	Reverse primer
Human-Calb1 (124bp)	AACTGAGATGGCCAGGTTAC	GTATCCATTGCCGTCCTGA
Human-GAPDH (95bp)	GATTCCACCCATGGCAAATT	TCTCGCTCCTGGAAGATGGT

The lenses from the same SD rat were promptly transferred into EP tubes containing 1.5 mL RNA later and stored at -20°C. After transferring the lenses into a 1.5mL EP tube, 700μL Lyse Buffer with 1% 2-mercaptoethanol in Purelink RNA extraction kit and an equal volume of 70% ethanol were added to facilitate tissue lysis. The tissue was then repeatedly sonicated for several seconds until no visible tissue block remained, followed by incubation on ice for 5 ~10 min. Subsequently, the lysate (700 μL) was loaded onto an elution column centrifuge tube and centrifuged at high speed (12,000 g) for 15 s at room temperature. This process was repeated to ensure complete transfer of the liquid. Next, Wash Buffer I (700 μL) was added to the elution column centrifuge tube, followed by another round of centrifugation at high speed for 15 s at room temperature to remove any residual contaminants. The elution tube was washed with Wash Buffer II (500 μL). After centrifuging at room temperature for 15 s, the liquid was discarded, and this step was repeated once more. To dry the elution column, it underwent another round of centrifugation at high speed for 1 min at room temperature before discarding both the collecting tube and liquid. A fresh collection tube replaced the previous one, and RNase-free Water (30 μL) was added to re-suspend RNA in the elution tube which then stood undisturbed for 1 min before being subjected to further centrifugation at high speed for 2 min. The resulting RNA-containing supernatant fluid was collected in a new collection tube.

After culturing HLECs 01/04 to cover over 80% of a 6-well plate, they were removed. The culture medium was discarded, and the cells adhered to the well walls were washed with PBS solution at 37°C for three consecutive times, each lasting 5 min. The cellular RNA extraction method remained consistent with the aforementioned procedure. Reverse transcription was conducted using a PCR-based system consisting of 20 μL reverse transcription reagents. The reaction conditions included reverse transcription at 37°C for 15 min, followed by inactivation at 85°C for 5 s. Finally, the resulting cDNA was stored at -80°C. For qRT-PCR amplification system, the following transcriptional reaction conditions were employed: initial denaturation at 96°C for 5 min followed by annealing at 60°C for 30 s; this cycle was repeated 35 times.

Establishment of the Selenium Cataract SD Rat Model

Healthy SD rats aged 8 d to 12 d, weighing approximately 20-25 g and with closed eyes, along with over 200 lactating rats of both genders, were randomly assigned to the control group or the selenium-induced cataract model group. The experimental time points were selected at 2 w, 4 w, 8 w, and 12 w. The SD rats in the selenium-induced cataract model group were initiated at the age of 12 d and subcutaneously injected with a volume of 0.2 ml of a sodium selenite saline solution containing a concentration of 2 mmol/L at the neck and back region. The maximum injection dose was administered every other day for three times, reaching a cumulative dose of approximately 230-250 μg.

Western Blot

Twelve SD rats with selenium-induced cataract at each time point (2w, 4w, 8w, and 12w) received individual abdominal anaesthesia using a dose of 2 ml of 3.6% chloral hydrate. After anaesthesia the intact lens was extracted by making an incision along the limbus of the eyeball and stored in groups at -80°C. Each lens was then transferred to a 1.5 mL EP tube and supplemented with a tissue lysis solution volume of 200 μL. Before usage, PMSF was added to reach a final concentration of 1 mM. The lens underwent multiple rounds of fine fragmentation and homogenization using an ultrasonic homogenizer until complete disruption occurred. Following centrifugation at speeds ranging from10-14 g for 3-5 min, the resulting supernatant was collected and stored in a refrigerator at -80°C. After HLECs 01/04 covered more than 80% of the area in a 6-well plate, they were removed. The culture medium was discarded, and the adherent cells on the well surface were rinsed three times with 37°C PBS solution for 5 min per rinse. The protein extraction method remained consistent as described above.

The absorbance at 562 nm was measured using a micro plate analyser, and the protein concentration was determined based on the standard curve. Subsequently, the protein concentration was adjusted to 5 mg/mL by diluting it with tissue lysate.

SDS-PAGE analysis was performed using a 5% stacking gel and a 12% separating gel. Equal volumes of protein samples (5 μL, corresponding to 20 μg of protein) were loaded into the sample wells. Electrophoresis was conducted at a constant pressure of 80 V until bromophenol blue dye reached the interface between the separating and stacking gels, followed by an increase in voltage to 120 V until the dye migrated to the bottom of the gel. Protein transfer onto a membrane occurred at a constant flow rate of 200 mA for 90 min, followed by washing with TBST for 5 min. The membrane was then blocked with skim milk powder (5%) at room temperature for 1 h, after which anti-CalB1 antibody (dilution: 1:3000) was added overnight at 4°C. Subsequent washes were performed using TBST for four cycles of 10 min each time. HRP-labeled secondary antibody (dilution: 1:20,000) incubation took place at room temperature for 1 h followed by additional washes with TBST and PBS to remove excess phosphate and Tween-20 respectively. Detection of proteins utilized Kangwei ECL luminescence kit combined with darkroom film exposure, while scanning quantitation involved measuring optical density from each strip.

Statistics

The statistical processing of data was conducted using the SPSS19.0 software package. Data were presented as $\bar{x}\pm s$, and comparisons between means were performed using one-way

ANOVA and independent sample t-test. A significance level of $p<0.05$ was considered to indicate a statistically significant difference.

Finding and Discussion

Effects of ion neomycin on the viability of HLECs and intracellular free Ca^{2+}

After treating HLECs with ionomycin at different concentrations for 1 h, the cell morphology of each group was observed under an inverted microscope and compared with that of the control group. Cell viability was assessed using CCK-8 assay, which revealed no significant difference among all groups after 1 h treatment with ionomycin ($p>0.05$) (Figure 1 A). However, as the concentration increased, high calcium spots were observed (Figure 2 B-E). Therefore, a concentration of 1.0μM ionomycin was determined to be the optimal treatment concentration.

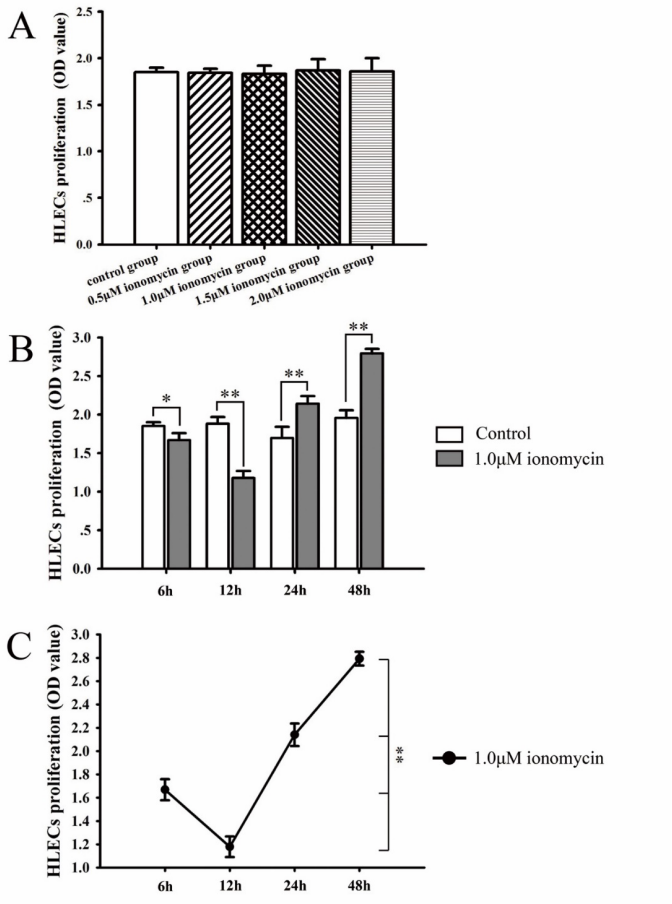

Figure 1: Effect of ionomycin on the viability of HLECs. A: No significant change in cell viability was observed after treatment with different concentrations of ionomycin for 1 hour, compared to the control group ($p>0.05$). B: HLECs were exposed to calcium overload using 1.0μM ionomycin. Cell viability decreased as intracellular Ca^{2+} concentration increased at 6 h and 12 h. At 12 h, cultured cells were switched to medium containing 1.0μM ionomycin. Cell viability did not further decline but instead increased at 24 h and 48 h. C: Calcium overload induced by 1.0μM ionomycin in HLECs exhibited a trend of initial decrease followed by an increase, reaching its lowest point at 12 h (*: $p<0.05$; **: $p<0.01$; n=8).

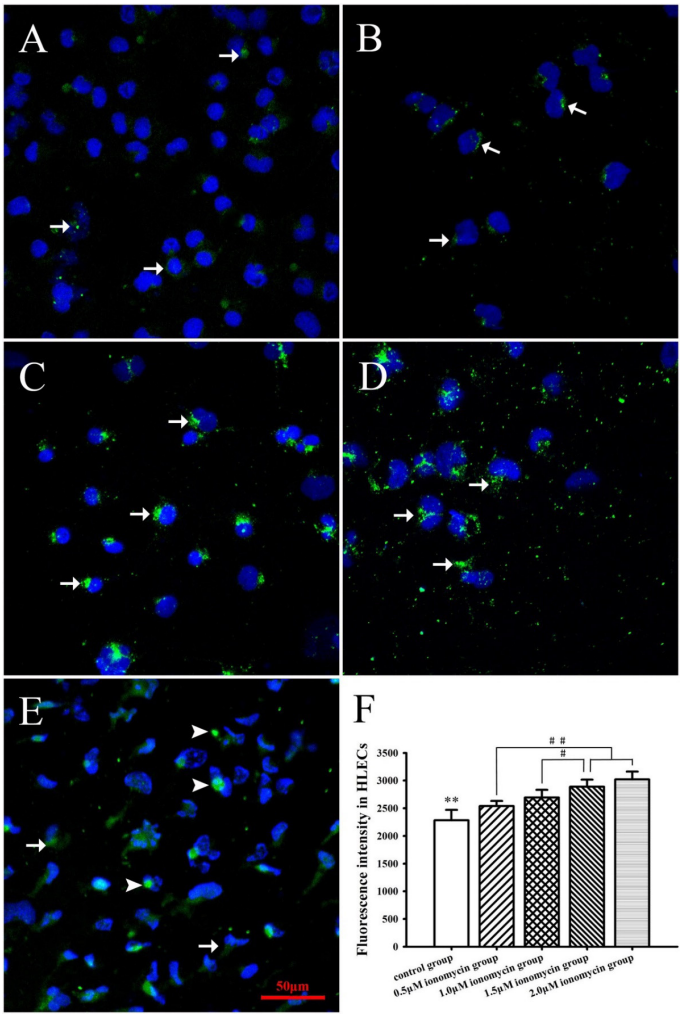

Figure 2: The localization of Ca^{2+} in the HLECs was investigated using a calcium fluorescence probe, Fluo-4 AM. After 1 h, slides of HLECs were treated with varying concentrations of ionomycin to assess its impact on Ca^{2+} distribution. Green fluorescence indicated the presence of Ca^{2+} (indicated by arrows), while nuclei were stained blue with DAPI. **A:** In the control group without ionomycin treatment, only a minimal amount of Ca^{2+} was observed in HLECs. **B:** Treatment with 0.5μM ionomycin resulted in a few small cytoplasmic spots. **C:** Moderate green staining spots appeared in the cytoplasm upon treatment with 1.0μM ionomycin. **D:** Treatment with 1.5μM ionomycin led to numerous flake-like staining areas. **E:** At an ionomycin concentration of 2.0μM, green staining areas aggregated into sporadic masses and caused disorganization of nuclei; this indicates that 2.0μM ionomycin can induce Ca^{2+} agglutination (filled arrowheads). **F:** The average fluorescence intensity levels in HLECs treated with different concentrations of ionomycin after 1h exhibited a concentration-dependent increase in intracellular Ca^{2+}. (**: $p<0.01$; ##: $p<0.01$; #: $p<0.05$; The scale bar represents 50μm; n=8.)

The HLECs were subjected to calcium ion overload using 1.0μM ionomycin, and the activity of HLECs was assessed at different time points. The results demonstrated that cell viability decreased with increasing intracellular Ca^{2+} concentration from 6 h to 12 h, compared to the control group. At 12 h, the culture medium was replaced with a medium containing 1.0μM ionomycin to maintain continuous intracellular Ca^{2+} overload. Interestingly, cell viability did not continue to decline but instead increased at 24 h and 48 h (Figure1 B). Following

ionomycin-induced Ca^{2+} overload in HLECs, cell viability initially decreased and then rebounded, reaching its lowest point at 12 h (Figure 1C).

The change in intracellular Ca^{2+} concentration in cultured HLECs was assessed using Fluo-4 as an indicator. Confocal microscopy was employed to qualitatively observe alterations in intracellular Ca^{2+} concentration (Figure 2 A-E). Fluorescence intensity of intracellular Ca^{2+} in HLECs was measured using a fluorimeter (Figure 3A), and the resulting values were used to quantify the intracellular Ca^{2+} concentration. In comparison to the control group, changes in intracellular Ca^{2+} concentration within the experimental group were found to be dependent on ionomycin concentration. Specifically, as ionomycin concentration increased, so did the level of Ca^{2+} within HLECs (Figure 2F). Intracellular Ca^{2+} overload was induced by 1.0μM ionomycin, and over time, its concentration gradually decreased and stabilized after 12 h (Figure 3B).

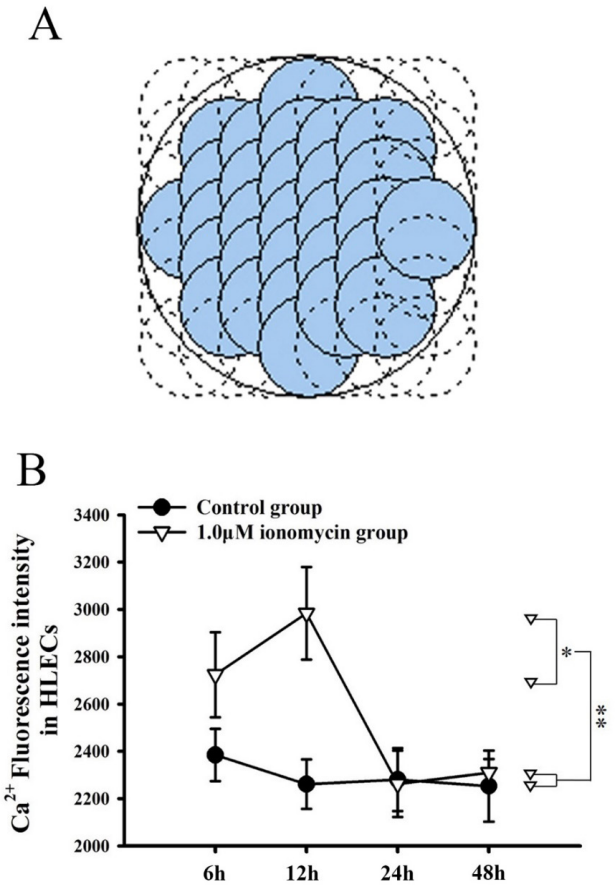

Figure 3A: The luciferase reader utilizes an equilateral matrix scanning pattern. It operates with an excitation wavelength of 494nm and an emission wavelength of 516nm. The optical element is positioned at the bottom, with a gain setting of 100. The detection speed is set to normal, and the detection height is 7mm. The scanning point consists of a grid size of 7×7, with a point spacing of 765μm × 765μm. The hole diameter measures at 6.6mm, while the probe diameter is 2.0mm. **B:** HLECs were induced to undergo intracellular calcium overload by treatment with ionomycin at a concentration of 1.0μM. Compared to the control group, there was a significant increase in intracellular Ca^{2+} levels observed at both the 6 h and 12 h time points; however, these levels returned to that of the control group after both the 24h and 48h time intervals (*: $p<0.05$; **: $p<0.01$; n=8).

Selenium-induced Cataract in a SD Rat Model

SD rats exhibited noticeable white nuclear opacity in the lens by 2 w after injection of sodium selenite (Figure 4B,b). By 4 w the nuclear opacity had expanded and the cortex became cloudy as the lens enlarged (Figure 4C,c). At 8 w, the white opacification area of the lens nucleus gradually decreased while transparency was restored to the cortex (Figure 4D,d). By 12 w, there was a gradual reduction in white opacities within the nucleus of the lens with partial restoration of transparency in some areas surrounding it (Figure 4E,e).

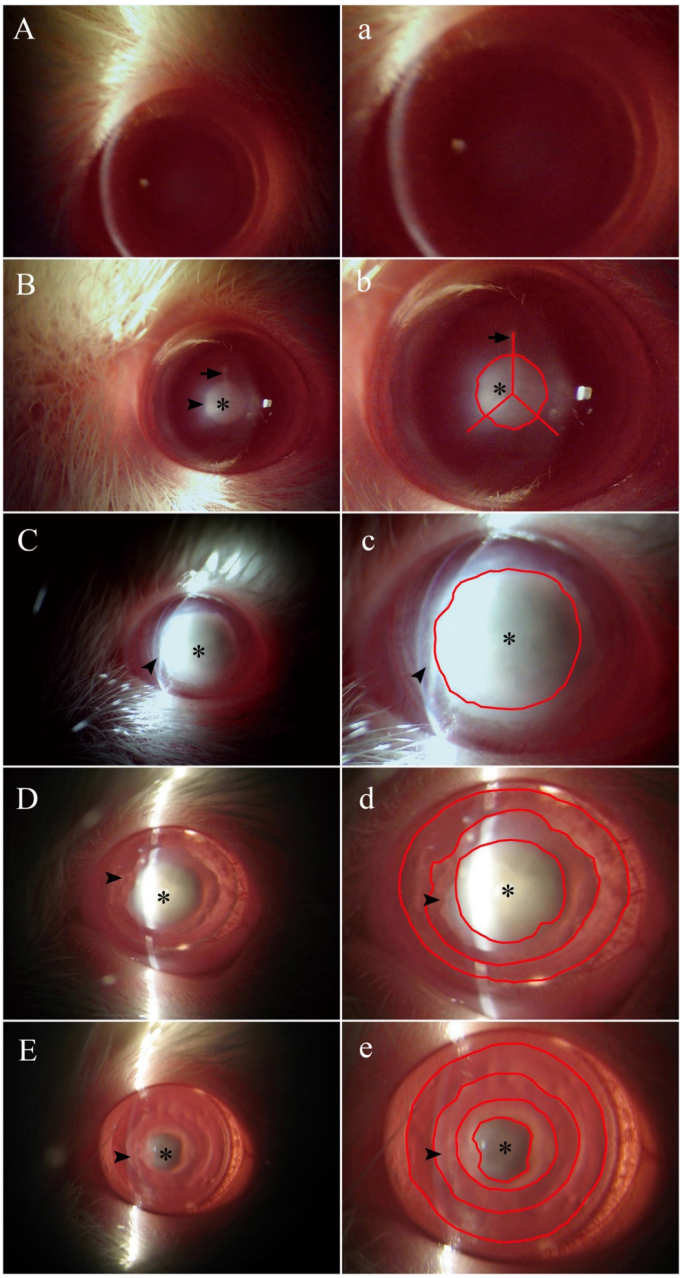

Figure 4: The control group consisted of SD rats without sodium selenite injection, and their lenses appeared transparent without any signs of turbidity (A and a). 2 weeks after sodium selenite injection, the lens of SD rats showed evident white nuclear opacity (indicated by arrow), as well as opacity in the "Y" slit of the lens (B and b). 4 weeks after sodium selenite injection, there was an enlargement in the scope of nuclear opacity within the lens, accompanied by cloudiness in the cortex (arrow) and expansion of the lens itself (C and c). 8 weeks after sodium selenite injection, the white opacification area in the nucleus region gradually decreased, while transparency was gradually restored

to the cortex (arrow) (D and d). 12 weeks after sodium selenite injection, further reduction in white opacities within the nucleus region was observed, with partial transparency appearing in some areas surrounding the lens cortex (arrow) (E and e). (* represents nucleus region of lens; pictures B-E and b-e are from same SD rat).

Immunohistochemistry of HLECs

The expression of Calb1 was observed in cultured normal HLECs (Figure 5F), and it exhibited a cytoplasmic distribution characterized by scattered and fine punctate staining patterns (Figure 5A). Following a 6 h calcium ion overload, the distribution of Calb1 in the cells started to decrease but remained dispersed throughout the cytoplasm, with diffuse areas showing positive Calb1 staining (Figure 5B). After 12 h, the number of Calb1 positive puncta in the cells began to increase again (Figure 5C). By 24 h, the fine punctate structure of intracellular Calb1 disappeared, and instead, scattered positive staining areas became concentrated near the nucleus with significantly enhanced fluorescence intensity compared to that at 6 h and 12 h (Figure 5D). At 48 h, intracellular distribution of Calb1 resembled that at 24 h; however, both fluorescence intensity and range were further increased and expanded compared to those at earlier time points (Figure 5E).

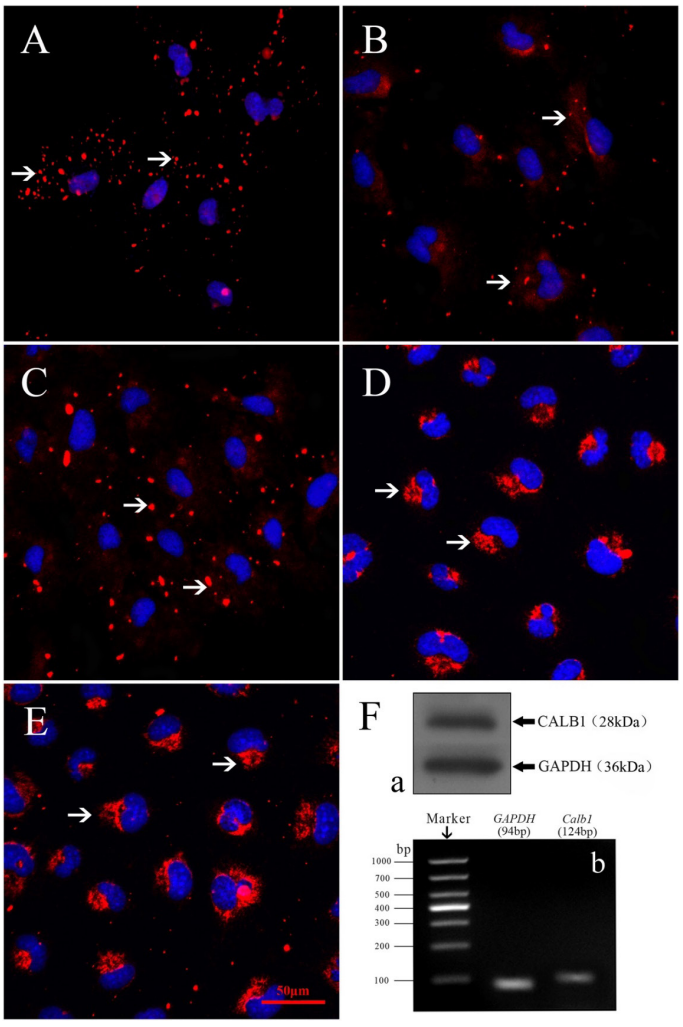

Figure 5: CALB1 protein distribution in HLECs at different time points following calcium overload was examined. A: In normal HLECs, CALB1 expression was observed in the cytoplasm of HLECs, appearing as scattered and fine staining (arrow). B: At 6h after calcium overload, the distribution of CALB1 in cells started to decrease and became more dispersed within the cytoplasm (arrow). C: At 12h after calcium overload, there was a reincrease in the number of microdot positive staining areas for intracellular CALB1 along with diffuse staining. D: At 24h after calcium overload, the microscopic structure of CALB1 disappeared from the cell and was replaced by concentrated diffuse positive staining areas near the nucleus (arrow). E: At 48h after calcium overload, CALB1 distribution in cells resembled that at 24h post-overload (arrow). F: Western blot bands and agarose gel electrophoresis bands were obtained from normal HLECs showing expression of CALB1 protein (a) and Calb1 mRNA (b). (The scale bar represents 50μm).

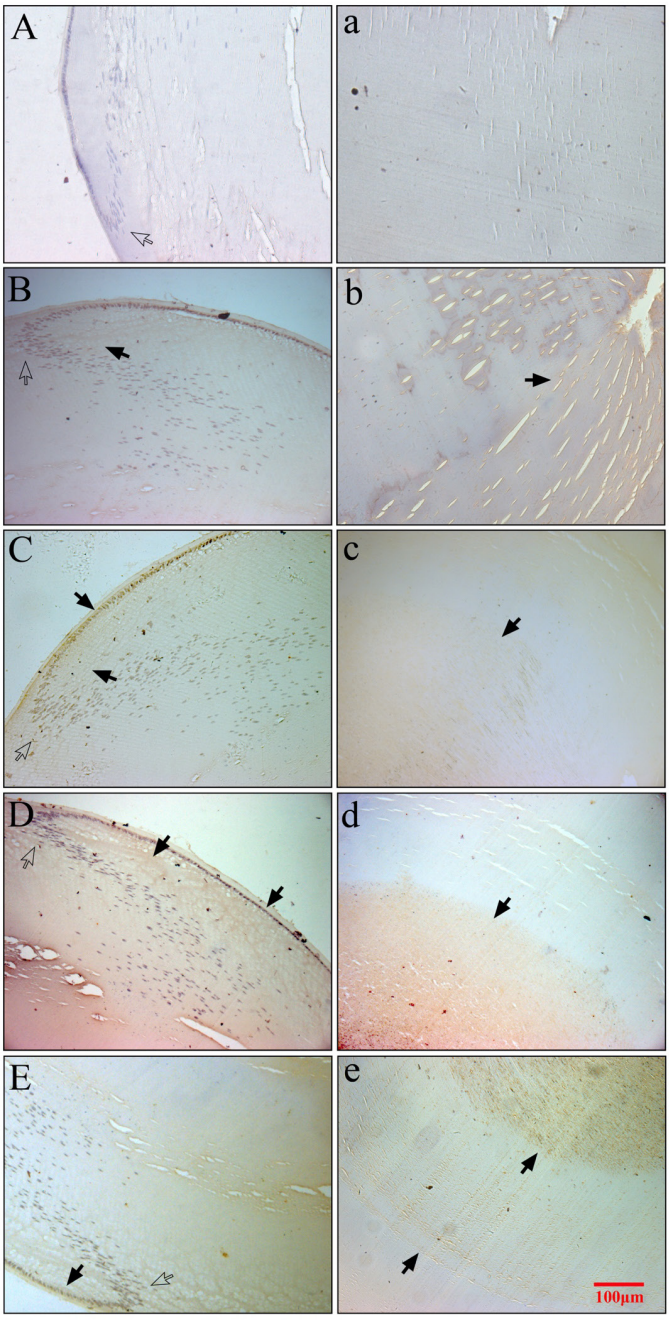

Figure 6: CALB1 protein expression distribution in the lens of selenium-induced cataract SD rats was examined. The left column (A-E) represents the cortex, while the right column (a-e) represents the nucleus. A and a: Control group; B and b: 2-week selenium-induced

cataract SD rats; C and c: 4-week selenium-induced cataract SD rats; D and d: 8-week selenium-induced cataract SD rats; E and e: 12-week selenium-induced cataract SD rats. Compared to the control group, CALB1 expression increased at each time point. At 8-week and 12-week, CALB1 expression showed significant localization within the internal nucleus region compared to the cortex-nucleus region, indicating clear demarcations. (The solid arrow indicates CALB1 positive staining area, while the hollow arrow indicates lens bow region; The scale bar represents 100μm).

In this experiment, DAB was employed to visualize the expression of Calb1 in the lens of selenium-induced cataract in SD rats. The findings revealed that, compared to the control group (Figure 6A,a), there was an upregulation of Calb1 expression in both the cortical and nuclear regions at 2 w post-injection (Figure 6B,b). Subsequently, at 4 and 8 w, Calb1 protein expression exhibited a gradual increase when compared to the levels observed at 2 w, predominantly within the nucleus but also extending into the cortex (Figure 6C-D and c-d). By 12 w, Calb1 distribution within the lens remained consistent with that observed at 8 w; however, notable compartmentalization of its expression became evident within the nuclear region with greater abundance towards its central portion as opposed to lateral areas (Figure 6E,e).

qRT-PCR

The expression levels of Calb1 mRNA in HLECs were measured after overloading with 1.0μM ionomycin for 6, 12, 24, and 48 h. Our results demonstrated that compared to the control group, there was no significant change in Calb1 expression at 6 h; however, it increased significantly at 12 h ($p<0.05$), showed a further significant increase at 24 h ($p<0.01$), and reached its peak at 48 h ($p<0.01$) (Figure 7 A).

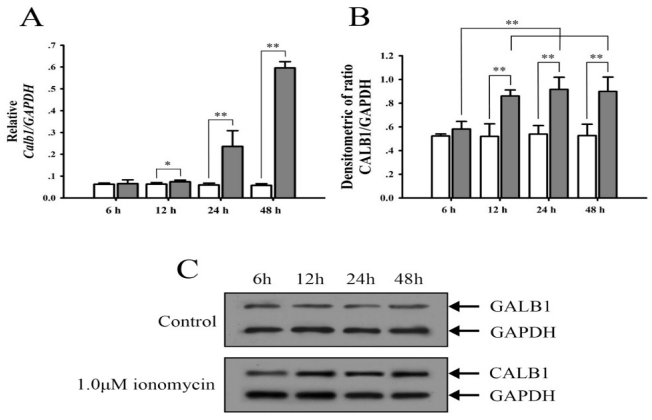

Figure 7: qRT-PCR and Western blot analyses were performed to investigate the changes in Calb1 expression. The results showed that after calcium overload with 1.0μM ionomycin, there was no significant change in Calb1 mRNA expression at 6h, but it increased at 12h, significantly increased at 24h, and peaked at 48h. Similarly, Western blot analysis revealed that the relative expression of CALB1 protein in HELCs did not change at 6h but increased significantly at later time points (12h, 24h and 48h) following calcium overload. (*: $p<0.05$, **: $p<0.01$, n=8)

In addition, the expression of Calb1 mRNA in lenses from selenium-induced cataract SD rats exhibited a gradual increasing trend compared to the control group at 2, 4, 8, and 12 weeks ($p<0.01$); however, Calb1 was down-regulated specifically at 12 weeks (Figure 8A, B).

Western Blot

The relative expression of Calb1 protein in HLECs was assessed at 6 h, 12 h, 24 h, and 48 h after calcium overload with 1.0μM ionomycin treatment. No significant changes were observed in the control group at any time point. In the experimental group, there was no change at 6 h but a significant increase in the relative expression level of Calb1 was observed at 12 h, 24 h, and 48 h ($p<0.01$) (Figure 7B, C).

The relative expression of Calb1 protein in the lens of selenium-induced cataract SD rats did not exhibit any significant changes at each time point in the control group. However, in the cataract model group, there was a significant decrease in Calb1 protein expression level at 2 weeks ($p<0.01$), followed by an increase at 4 weeks ($p<0.05$). Notably, Calb1 protein exhibited high expression levels at both 8 and 12 weeks ($p<0.01$) (Figure 8C, D).

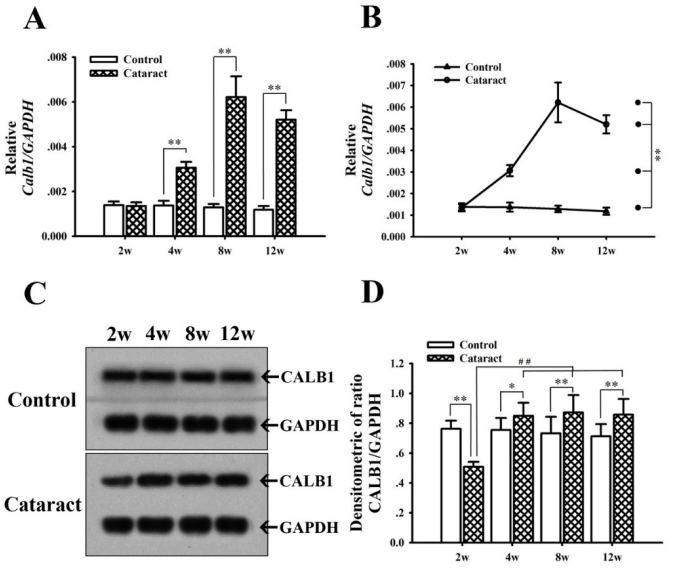

Figure 8: qRT-PCR and Western Blot analysis were performed to investigate the expression of Calb1 in the lens of rats with selenium-induced cataracts. A and B: qRT-PCR analysis revealed a significant up-regulation of Calb1 mRNA expression in the lens following cataract formation at 4 weeks, reaching its peak at 8 weeks, and slightly down-regulated at 12 weeks compared to the control group. C: Western Blot bands showed CALB1 (28kDa) bands along with GAPDH (36kDa) bands in both control and cataract groups at 2, 4, 8, and 12 weeks. D: Western Blot analysis demonstrated that there was no change in CALB1 protein expression in the lens of the control group throughout all time points. However, in selenium-induced cataract SD rats, CALB1 protein expression was significantly down-regulated at 2 weeks ($p<0.05$), followed by a significant up-regulation from 4 to 12 weeks which remained elevated (*: $p<0.05$, **: $p<0.01$, n=8).

Discussion

Calcium ions play a crucial role in numerous biological processes *in vivo*. Maintaining stable intracellular calcium levels and ensuring its proper distribution across the cell membrane are essential prerequisites for various vital activities

and signal transduction pathways. Disruption of intracellular calcium homeostasis can lead to cellular calcium overload, characterized by an abnormal increase in intracellular calcium concentrations up to 100 times higher than normal. Previous investigations have established a correlation between the occurrence and progression of human cataracts and aberrant elevation of lens calcium ion concentration [32-36].

In this study, the SRA01/04 exhibited functional characteristics similar to HLEC *in vivo*, enabling direct observation of HLECs' response to drugs and ion imbalances without the confounding influence of complex *in vivo* microenvironments. Additionally, an *in vitro* Ca^{2+} overload cell model was established using ionomycin, a highly specific calcium ion transporter for Ca^{2+} [37]. Ionomycin selectively binds calcium ions within pH 7.0-9.5 range and facilitates their entry into cells through the cell membrane. The transport mechanism may involve (1) transmembrane transport of extracellular calcium ions into intracellular space; (2) mobilization of intracellular calcium ion pool for release; (3) regulation of calcium ion storage capacity following depletion of intracellular calcium reservoirs [38]. Results demonstrated that different concentrations of ionomycin had no significant impact on cultured HLECs' viability after 1 h. Notably, 1.0μM concentration effectively increased intracellular Ca^{2+} levels in a concentration-dependent manner while avoiding excessive intracellular accumulation or formation of high calcium aggregates caused by higher concentrations of ionomycin use [39,40].

Our experiments demonstrated that following calcium overload, the CCK-8 tests conducted at 6 h and 12 h revealed a gradual decline in the viability of cultured HLECs with increasing degrees of calcium overload. However, at 24 h and 48 h, cell viability did not continue to decrease; instead, it increased proportionally with the degree of calcium overload. Additionally, we observed a significant increase in intracellular calcium ion fluorescence intensity at 6 h and 12 h, while the concentration of intracellular calcium ions decreased to levels comparable to those of the control group at 24 h and 48 h. Therefore, we propose that cells possess an autoregulatory mechanism after experiencing calcium overload which reduces intracellular calcium concentration and prevents excessive accumulation, thereby mitigating potential damage caused by elevated levels of calcium.

Previous studies have demonstrated the crucial role of calcium-binding proteins in maintaining intracellular calcium homeostasis and safeguarding cells against damage induced by calcium overload. Calb1, a member of the superfamily of calcium-binding proteins [41], exhibits widespread distribution throughout the body [42]. Our findings reveal the expression of Calb1 in HLECs, suggesting a potential association between the presence of Calb1 and the stability of Ca^{2+} levels within and outside the lens.

Calb1 exhibits a high affinity for calcium ions and rapidly binds to them in the body, thereby buffering the increase in calcium ion concentration. Immunofluorescence qualitative observation and analysis of Calb1 were performed on HLECs at different time points following calcium overload. It was observed that Calb1 predominantly localized in the cytoplasm of normal cells, displaying a characteristic star-like distribution pattern. However, upon 6 h of calcium overload, dot distribution of Calb1 decreased while diffuse staining areas with positive Calb1 signals emerged. After 12 h, spotty distribution of Calb1 started to increase again alongside persistent diffuse distribution which expanded to some extent. At 24 h, spotty distribution disappeared and was replaced by diffuse staining regions concentrated around or near the nucleus with enhanced fluorescence intensity. This trend continued at 48 h where diffusion area further expanded without significant change in fluorescence intensity compared to that at 24 h. Morphological analysis revealed regular changes in expression patterns of Calb1 in HLECs following Ca^{2+} overload.

The changes in intracellular Calb1 expression in HLECs at different time points after calcium overload were further confirmed through qRT-PCR and Western Blot analysis. The experimental results revealed a significant increase in Calb1 protein expression after 6 h, which was consistent with the mRNA level as indicated by qRT-PCR. Based on these findings, it can be speculated that Calb1 plays a crucial role in reducing and stabilizing intracellular calcium ion concentration following calcium overload.

The selenium cataract SD rat model is currently considered an ideal animal model for simulating senile cataract [29,30,43,44]. Sodium selenite-induced cataract in this model primarily involves calcium overload and oxidative damage [26], which reflects the pathological changes observed in senile cataracts to a certain extent [28]. Selenium cataracts can be induced in SD rats by subcutaneously administering a sodium selenite solution at a dose of 19-30μmol/kg on the neck and back between the ages of 10 to 14 d(window period) [27], with a cumulative dose not exceeding 600μg for selenium-induced cataract development [45]. Our experiment revealed that when the administered dose reached 390μg, the mortality rate among SD rats was nearly 100%. We observed typical nuclear cataracts occurring in suckling SD rats on the seventh day after completing modeling with a cumulative dose of 230μg. From 2 to 4 weeks, lens cortex turbidity successively occurred in these rats. After 4 weeks, total cataracts gradually formed without any deaths occurring. However, from 8 to 12 weeks, total cataracts gradually regressed as surrounding cortex became transparent and nuclear cataract areas shrank. This re-transparency may be attributed to lens self-repair ability; however, its mechanism remains unclear [46]. In our study using the selenium-induced rat model of cataracts, we found that Calb1 expression significantly decreased during early-stage formation but continued increasing thereafter and remained consistently high throughout further development and regression stages of the disease. Immunohistochemical experiments also demonstrated that Calb1 distribution within lenses of selenium-induced rat models correlated with opaque areas while exhibiting high expression levels during post-cataract formation regression phases. Based on these findings, we hypothesize that Calb1 plays a protective role.

We hypothesize that calcium homeostasis also plays a pivotal role in the pathogenesis of age-related cataract in humans, based on the findings from both *in vitro* and *in vivo*

experiments. The Calb1 protein serves as a crucial factor for maintaining intracellular calcium homeostasis. Although our study suggests potential involvement of Calb1 in cataract formation and progression, it falls short of elucidating the precise physiological function of Calb1 within the lens. Further investigations are warranted to unravel the specific regulatory mechanisms governing intracellular Ca^{2+} dynamics and its interactions with other cellular components.

Acknowledgments

This study was funded by the National Natural Science Foundation of China (No. 82360205). The sponsor had no involvement in the original study protocol design, data collection, analysis, interpretation, report writing or manuscript submission decision.

References

1. Hejtmancik JF, Kantorow M. Molecular genetics of age-related cataract. Exp Eye Res. 2004; 79(1): 3-9.
2. Celio MR, Heizmann CW. Calcium-binding protein parvalbumin as a neuronal marker. Nature. 1981; 293(5830): 300-302.
3. Heizmann CW, Braun K. Changes in Ca(2+)-binding proteins in human neurodegenerative disorders. Trends Neurosci. 1992; 15(7): 259-264.
4. Kennedy MB. Regulation of neuronal function by calcium. Trends Neurosci. 1989; 12(11): 417-420.
5. Malenka RC, Kauer JA, Perkel DJ, Nicoll RA. The impact of postsynaptic calcium on synaptic transmission--its role in long-term potentiation. Trends Neurosci. 1989; 12(11): 444-450.
6. Means AR, Tash JS, Chafouleas JG. Physiological implications of the presence, distribution and regulation of calmodulin in eukaryotic cells. Physiol Rev. 1982; 62(1): 1-39.
7. Pfyffer GE, Faivre-Bauman A, Tixier-Vidal A, Norman AW, Heizmann CW. Developmental and functional studies of parvalbumin and calbindin D28K in hypothalamic neurons grown in serum-free medium. J Neurochem. 1987; 49(2): 442-451.
8. Pfyffer GE, Humbel B, Strauli P, Mohrmann I, Murer H, et al. Calcium-binding proteins in carcinoma, neuroblastoma and glioma cell lines. Virchows Arch A Pathol Anat Histopathol. 1987; 412(2): 135-144.
9. Richard I, Broux O, Allamand V, Fougerousse F, Chiannilkulchai N, et al. Mutations in the proteolytic enzyme calpain 3 cause limb-girdle muscular dystrophy type 2A. Cell. 1995; 81(1): 27-40.
10. Sheetz MP, Steuer ER, Schroer TA. The mechanism and regulation of fast axonal transport. Trends Neurosci. 1989; 12(11): 474-478.
11. Hemmingsen C. Regulation of renal Calbindin-D28k. Pharmacol Toxicol. 2000; 87.
12. Duncan MJ, Franklin KM. Expression of 5-HT7 receptor mRNA in the hamster brain: effect of aging and association with calbindin-D28K expression. Brain Res. 2007; 1143: 70-77.
13. Iacopino AM, Rhoten WB, Christakos S. Calcium binding protein (calbindin-D28k) gene expression in the developing and aging mouse cerebellum. Brain Res Mol Brain Res. 1990; 8(4): 283-290.
14. Hall AK, Norman AW. Acute actions of 1,25-dihydroxyvitamin D3 upon chick pancreatic calbindin-D28K. Biochem Biophys Res Commun. 1991; 176(3): 1057-1061.
15. Margolis DS, Kim D, Szivek JA, Lai LW, Lien YH. Functionally improved bone in calbindin-D28k knockout mice. Bone. 2006; 39(3): 477-484.
16. Faucheux C, Bareille R, Amedee J. Synthesis of calbindin-D28K during mineralization in human bone marrow stromal cells. Biochem J. 1998; 333(3): 817-823.
17. Baimbridge KG, Celio MR, Rogers JH. Calcium-binding proteins in the nervous system. Trends Neurosci. 1992; 15(8): 303-308.
18. Celio MR. Calbindin D-28k and parvalbumin in the rat nervous system. Neuroscience. 1990; 35(2): 375-475.
19. Duncan G, Bushell AR. Ion analyses of human cataractous lenses. Exp Eye Res. 1975; 20(3): 223-230.
20. Iacopino AM, Christakos S. Specific reduction of calcium-binding protein (28-kilodalton calbindin-D) gene expression in aging and neurodegenerative diseases. Proc Natl Acad Sci U S A. 1990; 87(11): 4078-4082.
21. Ilg EC, Schafer BW, Heizmann CW. Expression pattern of S100 calcium-binding proteins in human tumors. Int J Cancer. 1996; 68(3): 325-332.
22. Marcantonio JM, Duncan G, Davies PD, Bushell AR. Classification of human senile cataracts by nuclear colour and sodium content. Exp Eye Res. 1980; 31(2): 227-237.
23. Jeon HK, Jin HS, Lee DH, Choi WS, Moon CK, et al. Proteome analysis associated with cadmium adaptation in U937 cells: identification of calbindin-D28k as a secondary cadmium-responsive protein that confers resistance to cadmium-induced apoptosis. J Biol Chem. 2004; 279(30): 31575-31583.
24. Johnson JA, Beckman MJ, Pansini-Porta A, Christakos S, Bruns ME, et al. Age and gender effects on 1,25-dihydroxyvitamin D3-regulated gene expression. Exp Gerontol. 1995; 30(6): 631-643.
25. Wernyj RP, Mattson MP, Christakos S. Expression of calbindin-D28k in C6 glial cells stabilizes intracellular calcium levels and protects against apoptosis induced by calcium ionophore and amyloid beta-peptide. Brain Res Mol Brain Res. 1999; 64(1): 69-79.
26. Hoenderop JG, Nilius B, Bindels RJ. Calcium absorption across epithelia. Physiol Rev. 2005; 85(1): 373-422.

27. Anderson RS, Shearer TR, Claycomb CK. Selenite-induced epithelial damage and cortical cataract. Curr Eye Res. 1986; 5(1): 53-61.

28. Mitton KP, Hess JL, Bunce GE. Causes of decreased phase transition temperature in selenite cataract model. Invest Ophthalmol Vis Sci. 1995; 36(5): 914-924.

29. Clark JI, Livesey JC, Steele JE. Delay or inhibition of rat lens opacification using pantethine and WR-77913. Exp Eye Res. 1996; 62(1): 75-84.

30. Hiraoka T, Clark JI, Li XY, Thurston GM. Effect of selected anti-cataract agents on opacification in the selenite cataract model. Exp Eye Res. 1996; 62(1): 11-19.

31. Tang D, Borchman D, Yappert MC, Vrensen GF, Rasi V. Influence of age, diabetes, and cataract on calcium, lipid-calcium, and protein-calcium relationships in human lenses. Invest Ophthalmol Vis Sci. 2003; 44(5): 2059-2066.

32. Hightower KR, Reddy VN. Ca++-induced cataract. Invest Ophthalmol Vis Sci. 1982; 22(2): 263-267.

33. Qian W, Shichi H. Cataract formation by a semiquinone metabolite of acetaminophen in mice: possible involvement of Ca(2+) and calpain activation. Exp Eye Res. 2000; 71(6): 567-574.

34. Nagai N, Ito Y, Takeuchi N. Correlation between hypersensitivity to hydrogen peroxide and low defense against Ca(2+) influx in cataractogenic lens of Ihara cataract rats. Biol Pharm Bull. 2011; 34(7): 1005-1010.

35. Yoshida H, Hirono C, Shimamoto C, Daikoku E, Kubota T, et al. Membrane potential modulation of ionomycin-stimulated Ca(2+) entry via Ca (2+)/H (+) exchange and SOC in rat submandibular acinar cells. J Physiol Sci. 2010; 60(5): 363-371.

36. Parekh AB, Penner R. Store depletion and calcium influx. Physiol Rev. 1997; 77(4): 901-930.

37. Purkiss JR, Willars GB. Ionomycin induced changes in intracellular free calcium in SH-SY5Y human neuroblastoma cells: sources of calcium and effects on [3H]-noradrenaline release. Cell calcium. 1996; 20(1): 21-29.

38. Melendez J, Welch S, Schaefer E, Moravec CS, Avraham S, et al. Activation of pyk2/related focal adhesion tyrosine kinase and focal adhesion kinase in cardiac remodeling. J Biol Chem. 2002; 277(47): 45203-45210.

39. Draznin B. Cytosolic calcium and insulin resistance. Am J Kidney Dis. 1993; 21(6): 32-38.

40. Espino J, Bejarano I, Paredes SD, Barriga C, Rodriguez AB, et al. Protective effect of melatonin against human leukocyte apoptosis induced by intracellular calcium overload: relation with its antioxidant actions. J Pineal Res. 2011; 51(2): 195-206.

41. Kojetin DJ, Venters RA, Kordys DR, Thompson RJ, Kumar R, et al. Structure, binding interface and hydrophobic transitions of Ca2+-loaded calbindin-D(28K). Nat Struct Mol Biol. 2006; 13(7): 641-647.

42. Duncan G, Wormstone IM. Calcium cell signalling and cataract: role of the endoplasmic reticulum. Eye. 1999; 13: 480-483.

43. Nabekura T, Tomohiro M, Ito Y, Kitagawa S. Changes in plasma membrane Ca2+ -ATPase expression and ATP content in lenses of hereditary cataract UPL rats. Toxicology. 2004; 197(2): 177-183.

44. Wang Z, Hess JL, Bunce GE. Deferoxamine effect on selenite-induced cataract formation in rats. Invest Ophthalmol Vis Sci. 1992; 33(8): 2511-2519.

45. Shearer TR, Ma H, Fukiage C, Azuma M. Selenite nuclear cataract: review of the model. Mol Vis. 1997; 3.

46. Shearer TR, David LL, Anderson RS, Azuma M. Review of selenite cataract. Curr Eye Res. 1992; 11(4): 357-369.